Hindawi
Shock and Vibration
Volume 2019, Article ID 3605830, 11 pages
https://doi.org/10.1155/2019/3605830

Research Article

Dynamic and Stability Analysis of the Machine Hydrostatic Slide with Magnetorheological Damper

Zhongkui Zhang,[1,2] **Feng Gao**,[1] **Yan Li**,[1] **and Han Zhang**[1]

[1]*Key Lab of NC Machine Tools and Integrated Manufacturing Equipment of the Education Ministry & Key Lab. of Manufacturing Equipment of Shaanxi Province, Xi'an University of Technology, Xi'an 710048, China*
[2]*Facility Horticulture Laboratory of Universities in Shandong, Weifang University of Science and Technology, Weifang 262700, China*

Correspondence should be addressed to Feng Gao; gf2713@126.com

Received 19 April 2019; Revised 30 June 2019; Accepted 17 July 2019; Published 1 August 2019

Academic Editor: Mahmoud Bayat

Tangential dynamic behaviors of the machine hydrostatic slide with a magnetorheological (MR) fluid damper are studied, and the effect of the MR damper to control the vibration of the hydrostatic slide is discussed. The dynamic model of the hydrostatic slide with the MR damper is established, and the tangential vibration equation of linear and nonlinear is derived. The multidimensional incremental harmonic balance method (MIHBM) with discrete Fourier transform (DFT) is derived by which the nonlinear response and stability of the system are studied. The resonance response of the Duffing equation under the combined action of harmonic excitation and constant excitation is obtained. In order to investigate the vibration response of the hydrostatic slide with the MR damper in detail, the bifurcation diagram, phase diagram, and Poincaré map are given. Finally, the dynamic response of the machine hydrostatic slide with the MR damper is discussed, and it is verified that the MR damper can suppress the tangential vibration of the hydrostatic slide effectively and the constant controller can control the chaotic behavior of the system well.

1. Introduction

A hydrostatic slide is widely used in precision machines because of the characteristic of low motion error and high stiffness [1, 2]. The normal vibration characteristics of the joint surface of the hydrostatic slide have been extensively studied by scholars at home and abroad [3–5]. The dynamic characteristics of the machine table is changed instantaneously and abruptly during the start-stop, acceleration to constant speed, and constant speed to deceleration because of the small friction coefficient and tangential low damping of the hydrostatic slide [6–8]. In addition, the system is forced to vibrate under the cutting force, ground vibration, residual vibration, and oil film nonlinear fluid fluctuation force which lead to poor stability of the hydrostatic slide in the tangential direction and will affect the positioning accuracy and work effectiveness. However, there are few research reports on the tangential vibration of the hydrostatic slide.

An MR damper and electrorheological (ER) damper are new intelligent vibration suppressors, which have widely been used in industrial and architectural fields in recent years. The magnitude of the force produced by the MR damper is mainly determined by the performance of internal MR fluid. The magnetorheological fluids are intelligent fluids which are very sensitive to magnetic field. When magnetic field is applied to magnetorheological fluids, the viscosity of magnetorheological fluids increases significantly and the MR fluid becomes viscoelastic solid [9]. The output damping force of the MR damper is regulated by input current. In a certain range, the greater the current, the stronger the electromagnetic field and the greater the output damping force. The working principle of the ER damper is similar to that of the MR damper. Kishore et al. [10] developed an electro-magnetorheological damper that can be used to control the process dynamics of the cutting tool and reduced cutting force by 12.9%. Tarng et al. [11] used a piezoelectric inertia actuator

which is mounted on the cutting tool to suppress chatter, and it was shown that chatter can be effectively suppressed. Fei et al. [12] experimentally verified the problem of the motion damper to suppress chatter in milling flexible parts. Hosseinabadi and Altintas [13] used active damping to effectively suppress the vibration of the machine tool and increase the bandwidth of the drive. Mori et al. [14, 15] proposed a passive viscoelastic damping system which can be applied to various machine tools to reduce the residual vibration. Aoyama and Inasaki [16] developed an electrorheological fluid damper which improved the stability of machine tool table systems with linear motion rolling element bearings. Chen [17] studied the dynamic characteristics of the linear feed system with the MR damper by virtual prototyping technology and proved the system has shorter positioning time, more stable speed characteristics, and better acceleration and deceleration characteristics. Bayat and Pakar [18–20] studied the nonlinear vibration response of beams using the Hamiltonian approach and variational approach, and it was demonstrated that two methods were very accurate and effective and therefore may find wide applicability in engineering and other sciences. In recent years, artificial neural networks were also developed for parameter identification and vibration prediction of nonlinear models [21, 22]. Most of the above studies improved the machining accuracy by suppressing tool chatter using dampers. However, vibration of the hydrostatic slide is also one of the important factors affecting the machining accuracy, and the influence of vibration of hydrostatic guide on processing accuracy has not been studied in the above literature.

In this paper, we studied the dynamic behaviors and stability of the machine hydrostatic slide with the magnetorheological damper. In the next section, the mathematical model of the machine hydrostatic slide with the magnetorheological damper was described and the tangential single-freedom dynamic model equations are derived. In Section 3, the MIHBM with DFT was derived and its accuracy is verified. Section 4 analyzed the linear and nonlinear dynamic responses and stability of the machine hydrostatic slide with the magnetorheological damper. Suppression of the vibration of the hydrostatic slide by using the magnetorheological damper is studied in detail in Section 5. Finally, some conclusions are drawn briefly in Section 6.

2. Dynamic Model of Hydrostatic Slide with MR Damper

In this section, the dynamic theoretical models of the MR damper and hydrostatic slide system were established, and the single-degree-of-freedom vibration equation of the hydrostatic slide with the MR damper is derived.

2.1. Design and Characterization of MR Damper. Figure 1 shows the structure of the MR damper, which is used to control the vibration of hydrostatic slide. According to the Bingham model of the MR damper [23, 24], the damping force F_{MR} is equivalent to the parallel connection of viscous damping force and Coulomb damping force, i.e.,

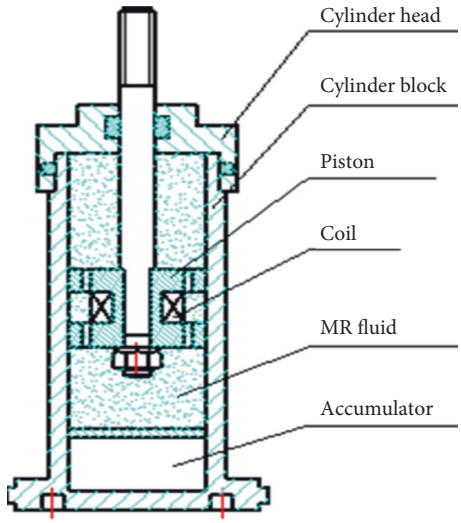

Figure 1: Structure of the MR damper.

$$F_{MR} = c_e v + F_I, \tag{1}$$

where c_e is the damping coefficient of MR fluid, F_I is the Coulomb damping force, and v is the relative velocity, which can be deduced by the structure of the magnetorheological damper:

$$c_e = \frac{12\eta A_p^2 l}{\pi D D_h^3},$$
$$\overline{F}_I = \frac{3lA_p}{D_h}\tau \operatorname{sgn}(v), \tag{2}$$

where l is the length of the piston, D is the inner diameter of the cylinder, A_p is the effective area of the piston, D_h is the diameter of the piston damping hole, τ is the yield shear stress, η is the viscosity coefficient, and sgn () is the symbolic function.

According to Ampere's loop law and magnetorheological fluid properties, the relationship between yield stress and current I is that

$$\tau = 1.43 \times 10^{-6}\left(\frac{\mu IN}{2h}\right)^2 + 4.743 \times 10^{-3}\left(\frac{\mu IN}{2h}\right) - 1, \tag{3}$$

where N is the number of coil, I is the input current, and u is the magnetic permeability of the magnetorheological fluid. The substitution of equations (2) and (3) into equation (1) yields

$$F_{MR} = \frac{12\eta A_p^2 l}{\pi D D_h^3} v + \frac{3lA_p}{D_h}\left(1.43 \times 10^{-6}\left(\frac{\mu IN}{2h}\right)^2 + 4.743 \times 10^{-3}\left(\frac{\mu IN}{2h}\right) - 1\right)\operatorname{sgn}(v). \tag{4}$$

The hysteresis three-dimensional model of the MR damper is obtained by parameter identification as shown in Figure 2.

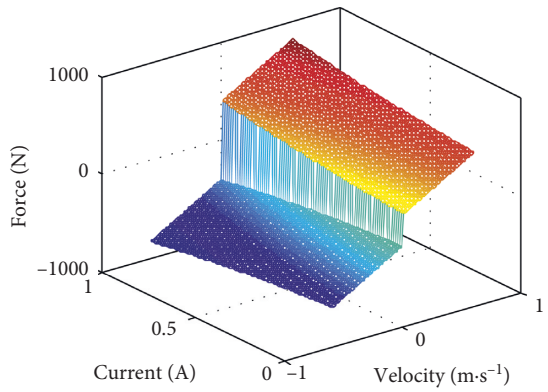

Figure 2: Hysteresis model of the MR damper.

Damping force increases with the increase of input current, but it does not increase linearly. When the current reaches 1.5 A, the output force tends to be saturated, which reflects the characteristics of nonlinear saturation of the MR damper. When the speed changes in different directions, the trajectory of the damping force is different, which reflects the hysteresis characteristics of the magnetorheological damper.

2.2. Dynamic Model of Hydrostatic Slide with MR Damper. The structure of the hydrostatic slide with the magnetorheological damper is shown in Figure 3. The cylinder of the MR damper is fixed. The damper rod is connected with the slide and generates damping force to control vibration of the worktable. The slide moves in the X direction, and the kinematics equation is as follows:

$$m\ddot{x} + F_c + F_s + F_f + F_L + F_{MR} = F_d, \tag{5}$$

where F_c is the structural damping force, F_s is the elastic force, F_f is the friction, F_L is the load, and F_{MR} is the driving force.

The structural damping force is affected by the material and internal resistance of the structure, i.e.,

$$F_c = c_1\dot{x}, \tag{6}$$

where c_1 is the structural damping coefficient. Assume that the friction is linear, i.e.,

$$F_c = c_2\dot{x}, \tag{7}$$

where c_2 is the linear friction coefficient.

In order to analyze the tangential dynamic characteristics of the hydrostatic slide with the magnetorheological damper, the system was simplified to the single-degree-of-freedom mechanical system model as shown in Figure 4. Let $F_d - F_L = \overline{F}\sin\overline{\omega}t$, and the vibration equation of the system is expressed as

$$m\ddot{x} + c\dot{x} + F_s(x) = \overline{F}\sin\overline{\omega}t - \overline{F}_I, \tag{8}$$

where $c = c_1 + c_2 + c_e$.

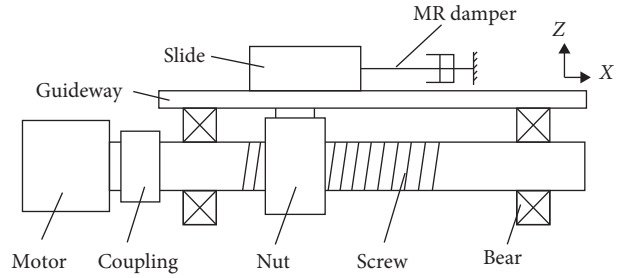

Figure 3: Structure of the hydrostatic slide system.

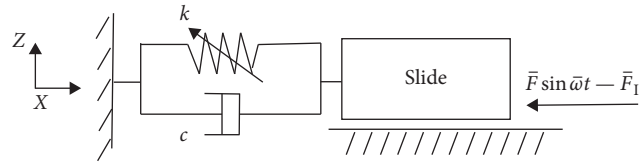

Figure 4: Single-degree-of-freedom mechanical system.

3. MIHBM with DFT Method and Feasibility Analysis

3.1. MIHBM with DFT. Wang et al. [25, 26] verified that the dynamic behaviors of the NC table have chaotic characteristics. So the system of the hydrostatic slide with the magnetorheological damper exhibits nonlinear properties. The elastic force [27]: $F_s = k_1x + k_3x^3$. Let $\tau = \overline{\omega}t$, $\omega_n = \sqrt{k/m}$, $\omega = \overline{\omega}/\omega_n$, $\zeta = c/2m\omega_n$, $F = \overline{F}/k_1$, and $F_I = \overline{F}_I/k_1$, dimensionless processing, the equation is transformed to

$$\omega^2x'' + 2\zeta\omega x' + x + \varepsilon x^3 = F\sin\tau - F_I, \tag{9}$$

where ε is the small parameter, $\varepsilon = k_3/k_1$, $0 < \varepsilon \le 1$.

MIHBM with DFT [28–32] is a new algorithm which replaces the Galerkin procedure [33, 34] with DFT. Equation (9) is a typical Duffing equation under the combined action of harmonic excitation and constant excitation. And the steady-state response of equation (9) is solved by the MIHBM with the DFT algorithm, which improves the computational efficiency.

Suppose x_0, ω_0 is the solution of the vibration equation, and increments are introduced as follows:

$$\begin{aligned} x &= x_0 + \Delta x, \\ \omega &= \omega_0 + \Delta\omega. \end{aligned} \tag{10}$$

By introducing equation (10) into equation (9) and omitting higher-order small quantities, the incremental equations with Δx and $\Delta\omega$ are obtained:

$$\begin{aligned} &\omega_0^2\Delta x'' + 2\zeta\omega_0\Delta x' + \left(1 + 3\varepsilon x_0^2\right)\Delta x \\ &\quad = F\sin\tau + F_I - \left(\omega_0^2x_0'' + 2\zeta\omega_0x_0' + x_0 + \varepsilon x_0^3\right) \\ &\quad -\left(2\omega_0x_0'' + 2\zeta\omega_0x_0'\right)\Delta\omega. \end{aligned} \tag{11}$$

The excitation $P(\tau)$, response $x_0(\tau)$, and its increment $\Delta x(\tau)$ can be expressed as the following Fourier series:

$$P(\tau) = F\sin\tau - F_I = \frac{p_0}{2} + \sum_{n=1}^{N}\left(p_{a_n}\cos(n\tau) + p_{b_n}\sin(n\tau)\right) = C_S P, \tag{12a}$$

$$x_0(\tau) = \frac{a_0}{2} + \sum_{n=1}^{N}\left(a_n\cos(n\tau) + b_n\sin(n\tau)\right) = C_S A_0, \tag{12b}$$

$$\Delta x(\tau) = \frac{\Delta a}{2} + \sum_{n=1}^{N}\left(\Delta a_n\cos(n\tau) + \Delta b_n\sin(n\tau)\right) = C_S \Delta A_0, \tag{12c}$$

where $C_S = (1\ \cos\tau\ \sin\tau \cdots \cos N\tau\ \sin N\tau)$, $P = (F_I\ \ 0\ \ F \cdots 0\ \ 0)^T$, $A_0 = ((a_0/2)\ \ a_1\ \ b_1 \cdots a_N\ \ b_N)$, $\Delta A = ((\Delta a_0/2)\ \ \Delta a_1\ \ \Delta b_1\ \cdots\ \Delta a_N\ \ \Delta b_N)^T$, and N is the number of harmonics.

According to reference [35], C_S is discretized to a matrix Γ and introducing the differential operator matrix D as follows:

$$\Gamma = \begin{pmatrix} 1 & \cos\tau_0 & \sin\tau_0 & \dots & \cos N\tau_0 & \sin\tau_0 \\ 1 & \cos\tau_1 & \sin\tau_1 & \dots & \cos N\tau_1 & \sin\tau_1 \\ \vdots & \vdots & \vdots & \vdots & \vdots & \vdots \\ 1 & \cos\tau_{i-2} & \sin\tau_{i-2} & \dots & \cos N\tau_{i-2} & \sin\tau_{i-2} \\ 1 & \cos\tau_{i-1} & \sin\tau_{i-1} & \dots & \cos N\tau_{i-1} & \sin\tau_{i-1} \end{pmatrix},$$

$$D = \begin{pmatrix} 0 & & & & & \\ & 0 & 1 & & & \\ & -1 & 0 & & & \\ & & & 0 & 2 & \\ & & & -2 & 0 & \\ & & & & & \ddots \\ & & & & & & 0 & N \\ & & & & & & -N & 0 \end{pmatrix}, \tag{13}$$

where i is the number of the data points in a period. So the incremental equation (11) can be expressed as

$$\begin{aligned} &\omega_0^2\Gamma D^2\Delta A + 2\zeta\omega_0\Gamma D\Delta A + \left(k_1 + 3k_3(\Gamma A_0)^2\right)\Gamma \\ &\quad = \Gamma P - \left(\omega_0^2\Gamma D^2 A_0 + 2\zeta\omega_0\Gamma D A_0 + k_1\Gamma A_0 + k_3(\Gamma A_0)^3\right) \\ &\qquad - \left(2\omega_0^2\Gamma D^2 A_0 + 2\zeta\Gamma D A_0\right)\Delta\omega, \end{aligned} \tag{14}$$

When equation (14) is multiplied by transpose matrix Γ^T, the following linearized incremental equation is obtained:

$$K_T\Delta A = R_m\Delta\omega + R, \tag{15}$$

where $K_T = \omega_0^2\Gamma^T\Gamma D^2 + 2\zeta\omega_0\Gamma^T\Gamma D + \Gamma^T(k_1 + 3k_3(\Gamma A_0)^2)\Gamma$, $R_m = -(2\omega_0\Gamma^T\Gamma D^2 A_0 + 2\zeta\Gamma^T\Gamma D A_0)$, $R = \Gamma^T\Gamma P - (\omega_0^2\Gamma^T\Gamma D^2 A_0 + 2\zeta\omega_0\Gamma^T\Gamma D A_0 + \Gamma^T(k_1\Gamma A_0 + k_3(\Gamma A_0)^3))$, and K_T, R_m, and R are the Jacobian matrix, unbalance force matrix, and corrective matrix, respectively.

Adding the constraint equation by the arc length method [31, 35]:

$$\Delta A^T\Delta A = \Delta l^2, \tag{16}$$

where Δl is the arc length parameter. Figure 5 shows the flow chart of the algorithm.

3.2. Feasibility Analysis of MIHBM with DFT. In order to verify the exactness and accuracy of the method proposed in the previous section, Figure 6 shows a comparisons between the approximate analytical solutions based on the MIHBM with DFT and the numerical results based on the Runge–Kutta methods. The vibration waveform and phase diagram of primary resonance response with $F = 0.5$, $F_I = 0.006$, and $\omega = 1.0$ of the hydrostatic slide with the MR damper are shown in Figure 6. NMM represents the numerical results based on the Runge–Kutta method. As demonstrated, the differences between both methods are very slight, so the MIHBM with DFT is feasible to analyze the dynamic behaviors of the hydrostatic slide with the MR damper.

4. Dynamic and Stability Analysis of Hydrostatic Slide with MR Damper

In this section, the dynamic behaviors and stability of the hydrostatic slide with the MR damper were studied by MIHBM with DFT.

4.1. Linear System Analysis. Assume the stiffness of the hydrostatic slide is much greater so that it can be regarded as a constant, namely, $F_s = k_1 x$. Thus, the hydrostatic slide can be regarded as a linear system. Let $\tau = \overline{\omega}t$, $\omega_n = \sqrt{k/m}$, $\omega = \overline{\omega}/\omega_n$, $\zeta = c/2m\omega_n$, $F = \overline{F}/k_1$, and $F_I = \overline{F}_I/k_1$, dimensionless processing, the equation is transformed to

$$\omega^2 x'' + 2\zeta\omega x' + x = F\sin\tau - F_I. \tag{17}$$

The steady-state response of equation (17) is

$$x(\tau) = \frac{F}{\sqrt{(1-\omega^2)^2 + (2\zeta\omega)^2}}\sin(\tau - \varphi) - F_I, \qquad \varphi = \arctan\frac{2\zeta\omega}{1-\omega^2}. \tag{18}$$

Figure 7 shows the vibration response.

The larger the Coulomb damping force F_I, that is, the greater the output force of the magnetorheological damper, the better the vibration suppression effect. When $F_I = 1.2$, the hydrostatic slide reaches a stable state quickly. However, it is known that the force produced by magnetorheological damping tends to be saturated when the current increases to a certain value.

The force produced by magnetorheological damping has a maximum value and cannot be increased indefinitely. The amplitude-frequency curve linear system shows that the

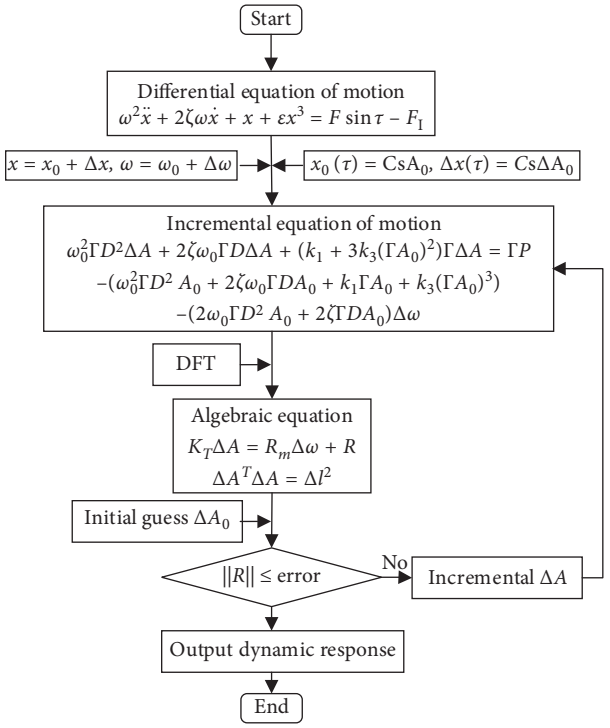

Figure 5: Algorithm of the MIHBM with DFT.

larger the damping coefficient, the smaller the amplitude of the system, as shown in Figure 8. Therefore, the viscous damping force of the MR damper can also reduce the vibrate displacement of the hydrostatic slide.

4.2. Effect of MR Damper on Amplitude-Frequency. Combined action of harmonic excitation and constant excitation is a prominent feature of vibration equation (9). In this subsection, the effects of constant excitation Coulomb force on the response of system are investigated using the amplitude-frequency curves. Let $\xi = 0.015$, $\varepsilon = 1$, and $F = 0.05$, for $F_I = 0.2$, 0.6, 0.9, 1.1, 1.2, 2.0, respectively, and the amplitude-frequency responses of the system are shown in Figure 9.

It can be seen from Figure 9(a) that the amplitude-frequency curve of the vibration system shows complete hardening-type nonlinearity when $F_I = 0.2$. With the increase in Coulomb damping force F_I to 0.9, the amplitude-frequency curve of the vibration system not only shows hardening-type nonlinearity but also exhibits slight softening-type nonlinearity. However, there is no overlap region between hardening-type nonlinearity and softening-type nonlinearity when $F_I = 0.9$. The amplitude-frequency curve of the vibration system show hardening-type nonlinearity and softening-type nonlinearity when $F_I = 1.1$, and there is overlap region between hardening-type nonlinearity and softening-type nonlinearity. When $F_I = 1.2$, the region of the softening-type nonlinearity covers the region of hardening-type nonlinearity completely. The amplitude-frequency curve of the vibration system shows the softening-type nonlinearity and slight hardening-type nonlinearity.

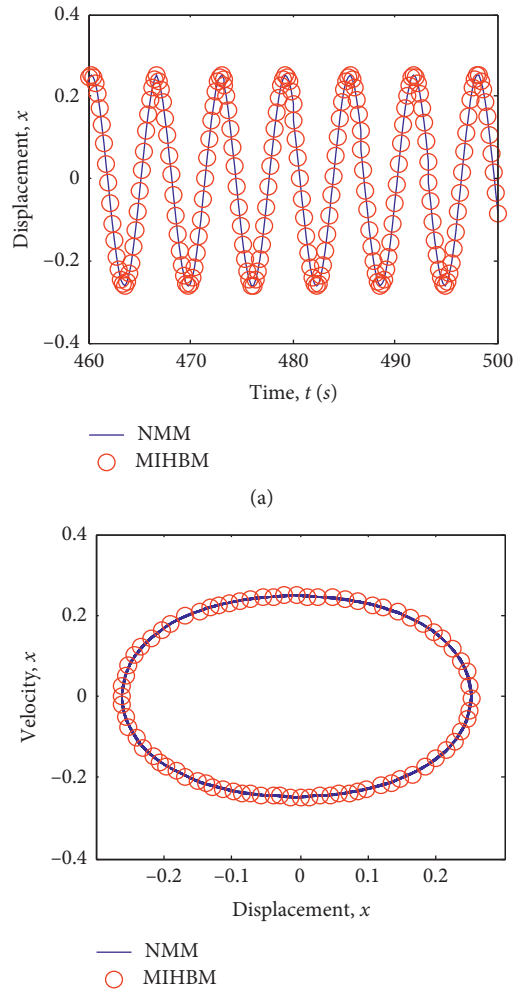

Figure 6: Vibration waveforms and phase diagrams.

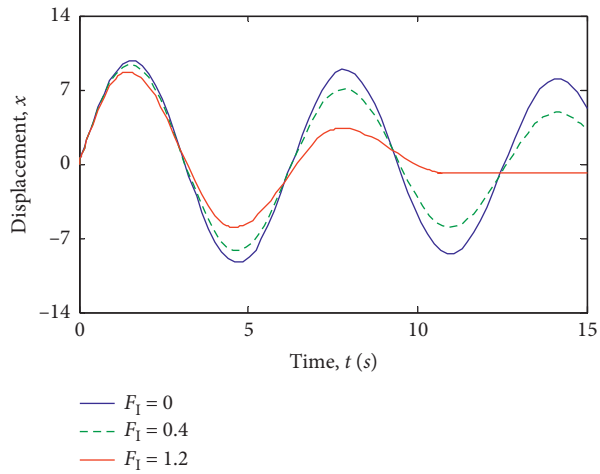

Figure 7: Vibration displacement at $F_I = 0$, 0.4, and 1.2.

With the increase in Coulomb damping force F to 2.0, hardening-type nonlinearity of the amplitude-frequency curve of the vibration system disappears completely

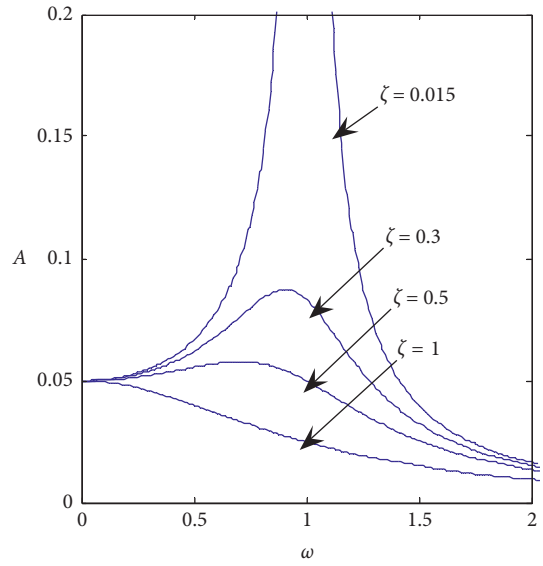

Figure 8: Amplitude-frequency curve.

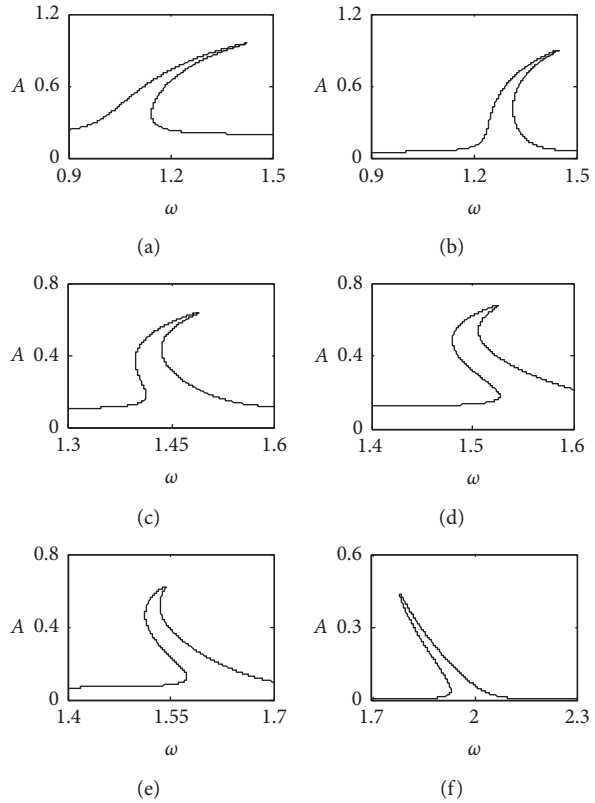

Figure 9: Amplitude-frequency curve. (a) $F_I = 0.2$, (b) $F_I = 0.6$, (c) $F_I = 0.9$, (d) $F_I = 1.1$, (e) $F_I = 1.2$, and (f) $F_I = 2.0$.

and the vibration system exhibits softening-type nonlinearity.

4.3. Dynamic and Stability Analysis of the Hydrostatic Slide with MRD. The Floquet method [36, 37] is an effective method to determine whether the periodic solution of a nonlinear dynamic system is stable. The periodic solution x_0 of the equation is obtained by MIHBM with the DFT method, and by substituting it into equation (11), the following equation is obtained:

$$\omega^2 \Delta x'' + 2\zeta\omega_0 \Delta x' + \Delta x + 3\varepsilon x_0^2 \Delta x = 0. \tag{19}$$

Introduce

$$X = \left[\Delta x, \Delta x'\right]^T,$$

$$Q(\tau) = \begin{bmatrix} 0 & 1 \\ -\dfrac{1 + 3\varepsilon x_0^2}{\omega_0^2} & \dfrac{-2\zeta}{\omega_0} \end{bmatrix}. \tag{20}$$

Equation (20) can be rewritten as

$$X' = Q(\tau)X. \tag{21}$$

According to the Hsu method proposed by Friedmann et al. [38], periodic T is divided into q_k equal-length subintervals and interval size is

$$\Delta k = \tau_k - \tau_{k-1} = \frac{T}{q_k}. \tag{22}$$

The state transition matrix of equation (20) is

$$\Phi = \prod_{j=q_k}^{1} \exp\left(Q_k \Delta_k\right) = \prod_{j=q_k}^{1} \left[I + \sum_{i=1}^{q_i} \frac{\left(\Delta_k Q_k\right)^i}{i!} \right], \tag{23}$$

where I is the unit matrix and q_i is the number of the polynomial expanded by the exponential matrix.

The eigenvalues λ_1 and λ_2 of matrix Φ are the Floquet multipliers of the system. If the modulus of all the Floquet multipliers of the system is less than 1, the solutions are stable and unstable otherwise. Moreover, if a real Floquet multiplier passes through the unit circle along the negative real axis and the rest are located in the unit circle, there is period-doubling bifurcation.

In this subsection, the steady-state solution of the hydrostatic slide with the magnetorheological damper system is studied by the Floquet method. Figure 10(a) shows the amplitude-frequency curve for $F_I = 1.1$, and it exhibits hardening-type nonlinearity and softening-type nonlinearity in different regions. And there is overlap region between hardening-type nonlinearity and softening-type nonlinearity. Each frequency value of the overlap region corresponds to five amplitude solutions, three of which are stable and two of which are unstable, and stable and unstable solutions alternate. At the lower excitation frequency (i.e., $\omega \in [0, 1.5269]$), the change of the vibration system steady response is very slight until the limit point at "2" ($\omega = 1.5269$). With the decrease in frequency ω, the amplitude A becomes unstable until the second limit point reaches "7" ($\omega = 1.4803$). By further increasing the frequency ω, the amplitude of the stable response increases obviously and the response amplitude reaches the peak value at point "9" ($\omega = 1.5237$). With the decrease in frequency ω, the vibration system becomes

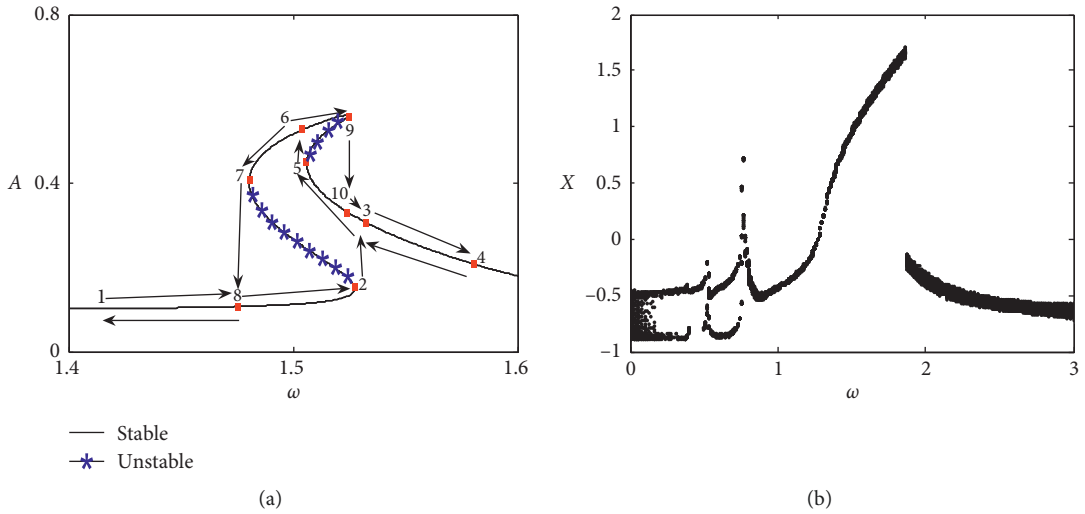

Figure 10: Nonlinear responses of the vibration system: (a) amplitude-frequency curves and (b) bifurcation diagram.

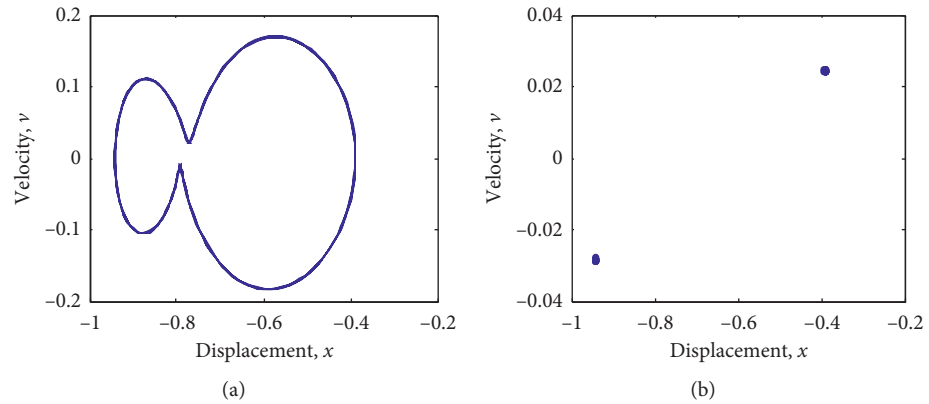

Figure 11: Dynamic response of the system at $\omega = 0.5$. (a) Phase diagram. (b) Poincaré map.

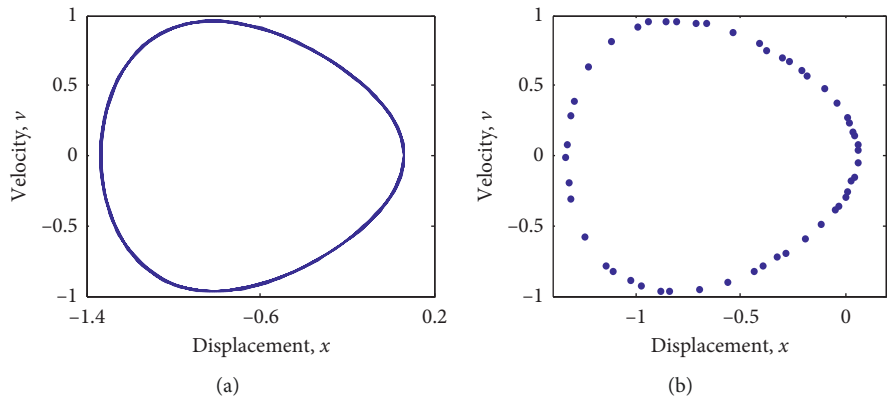

Figure 12: Dynamic response of the system at $\omega = 1.29$. (a) Phase diagram. (b) Poincaré map.

unstable until the point at "5" ($\omega = 0.5052$). Then, the vibration system returns to stable response once again.

With the increase of the excitation frequency ω from point "1" to point "4," the path of the stable response is $1 \longrightarrow 2 \longrightarrow 3 \longrightarrow 4$. There appears the jumping phenomenon of stable solutions, and the point "2" is the jumped point. With the increase of the excitation frequency from point "4" to point "1", the path of the stable response is $4 \longrightarrow 5 \longrightarrow 6 \longrightarrow 7 \longrightarrow 8 \longrightarrow 1$. There appears the jumping phenomenon of stable solutions, and the points "5" and "7"

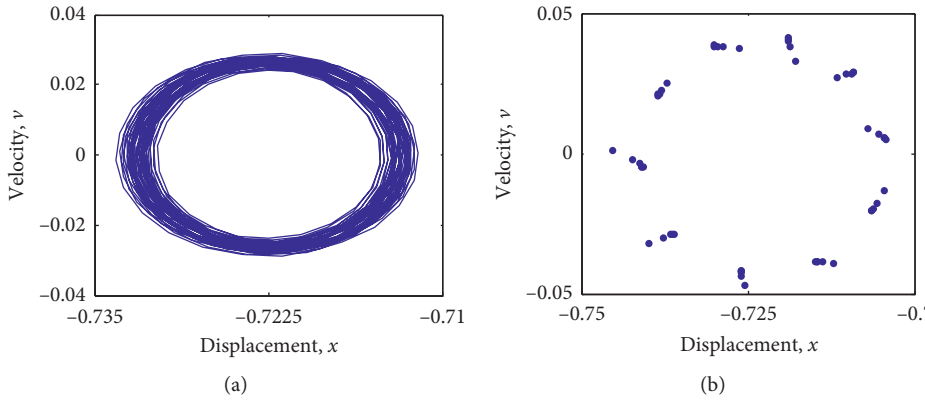

Figure 13: Dynamic response of the system at $\omega = 2.8$. (a) Phase diagram. (b) Poincaré map.

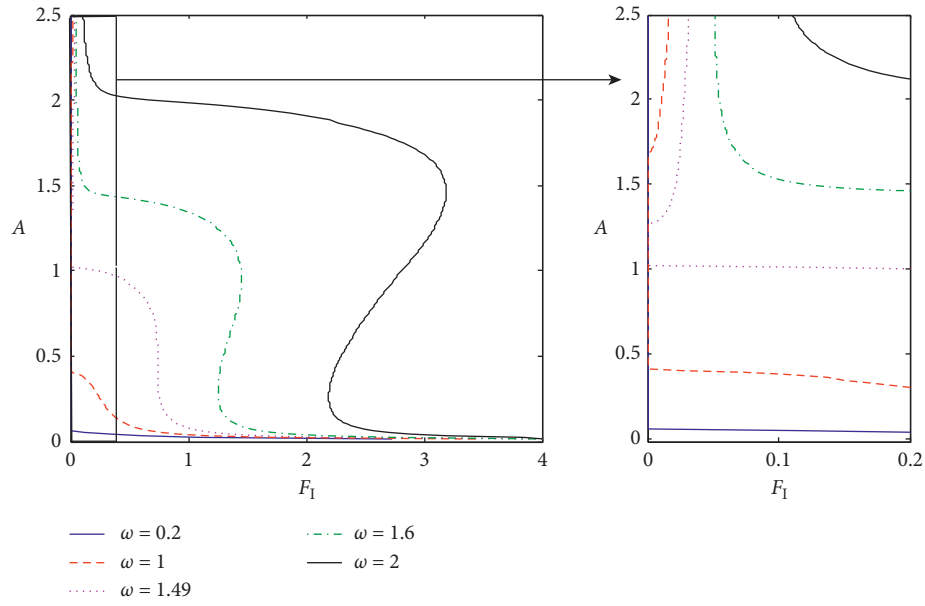

Figure 14: Amplitude-force curves of the system.

are jumped points. The stable solution between points "6" and "9" is achieved by the path $4 \longrightarrow 5 \longrightarrow 6 \longrightarrow 9 \longrightarrow 10 \longrightarrow 4$, and the jumped points are "5" and "9."

Figure 10(b) presents the bifurcation diagram of the hydrostatic slide with the magnetorheological damper system with the parameter ω. At the lower excitation frequency (i.e., $\omega \in [0, 0.06]$), the vibration system exhibits chaos motion. In the range of $\omega \in [0.06, 1.87]$, the vibration system exhibits various types of motion including periodic-n and chaotic motions, as shown in Figures 11 and 12. With the increasing of excitation frequency, the vibration system exhibits chaos motion again in the range of $\omega \in [1.87, 3]$, as shown in Figure 13.

5. The Effect of MR Damper to Control Vibration of Hydrostatic Slide

The relationship between amplitude A and constant excitation Coulomb damping force F_I is shown in Figure 14. For $\omega = 0.2, 1, 1.49, 1.6, 2.0$, respectively, the $A - F_I$ curve is quite different. At lower Coulomb damping force, there appears the jumping phenomenon of stable solutions. With the increase of Coulomb damping force F_I, the amplitude decrease monotonously for the curve $\omega = 0.2$, 1, 1.49, respectively. The fact is that the $A - F_I$ curve decreases monotonously as long as $\omega \leq 1.49$. Moreover, the amplitude A decreases rapidly when Coulomb damping force F_I increases to a certain value as shown in Table 1. By further increasing Coulomb damping force F_I, the amplitude tends to zero for the curve $\omega = 0.2$, 1, 1.49, respectively. However, there appears the jumping phenomenon of stable solutions for the curve of $\omega = 1.6$ and 2. It can be seen from the above analysis that the MR damper can reduce the vibration amplitude of the hydrostatic slide effectively.

Figure 15(a) presents the bifurcation diagram of the hydrostatic slide with the magnetorheological damper system with the parameter F_I. The system exhibits chaotic motion after a very short period-doubling bifurcation. With

Table 1: Comparison of amplitude corresponding to $F_I = 0.1, 0.2, 0.5, 1, 2, 3.5$.

Case	Vibration amplitude of system					
	$F_I = 0.1$	$F_I = 0.2$	$F_I = 0.5$	$F_I = 1$	$F_I = 2$	$F_I = 3.5$
$\omega = 0.2$	0.051	0.046	0.055	0.019	0.014	0.009
$\omega = 1$	0.370	0.309	0.121	0.037	0.018	0.010
$\omega = 1.49$	1.012	1.002	0.953	0.077	0.023	0.013
$\omega = 1.6$	1.527	1.458	1.445	1.355	0.036	0.016
$\omega = 2$	2.681	2.113	2.049	1.975	1.904	0.017

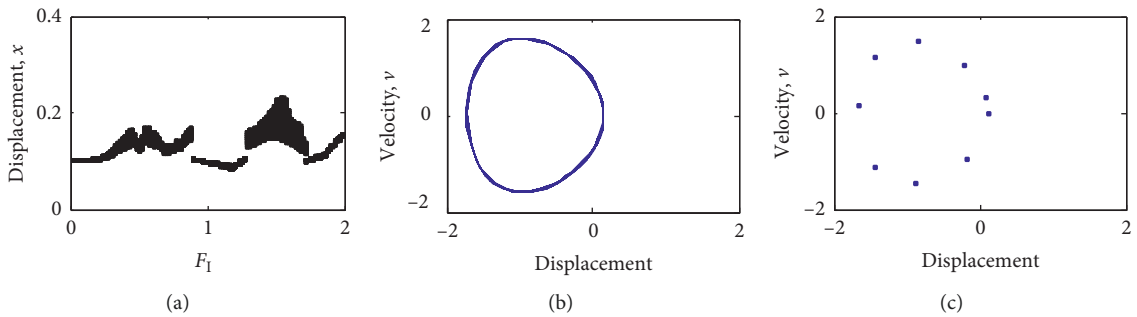

Figure 15: Dynamic response of the system. (a) Bifurcation diagram. (b) Phase diagram. (c) Poincaré map.

an increase in F_I, the vibration system displays period-doubling bifurcation again in the interval [0.76, 1.09]. When $F_I > 1.47$, the system present period-doubling bifurcation stably. Figures 15(b) and 15(c) present the phase diagrams and Poincaré diagrams, respectively, when $F_I = 1.7$. It can be seen that the constant controller can control the chaotic behavior of the system well, which is consistent with that conclusion [39]. So the effect on the magnetorheological damper to control the vibration of the hydrostatic slide is excellent.

6. Conclusions

In this paper, the tangential dynamic characteristics and stability of the machine hydrostatic slide with the MR damper are studied by using a single-freedom dynamic model. The nonlinear responses the vibration equation are calculated using the IHBM with DFT, and the stability of the solutions is checked using the Floquet method. Finally, the effect of the MR damper to control the vibration of the hydrostatic slide is discussed, and it is verified that the constant controller can control the chaotic behavior of the system well.

(1) The MIHBM with DFT is derived which is proven to be feasible to analyze nonlinear dynamic behavior.

(2) For the machine hydrostatic slide with the MR damper, the hardening- and softening-type nonlinearities are observed in amplitude-frequency curves. There is an overlap region between hardening-type nonlinearity and softening-type nonlinearity when $F = 1.1$ and each frequency value of the overlap region corresponds to five amplitude solutions. With the increase in frequency, hardening-type nonlinearity disappears completely and the vibration system exhibits softening-type nonlinearity. In addition, the maximum amplitude of the machine hydrostatic slide with the MR damper decreases obviously.

(3) The bifurcation diagram, phase diagram, and Poincaré map for the vibration system under different excitation frequency are illustrated. With the increasing excitation frequency, the vibration system exhibits more complex dynamic behaviors including wide variety of period motion, chaotic behavior motion, and jumping discontinuous phenomena.

(4) The appropriate damping force provided by using the MR damper can reduce the tangential vibration of the hydrostatic slide effectively.

(5) Constant controller can control the chaotic behavior of the Duffing system well.

Overall, the researches in this paper can not only understand the dynamic response of the machine hydrostatic slide with the MR damper but also provide some reference to suppress vibration and design and optimize the vibration system.

Data Availability

The data used to support the findings of this study are included within the article.

Conflicts of Interest

The authors declare that there are no conflicts of interest regarding the publication of this paper.

Acknowledgments

This work was financially supported by the National Natural Science Foundation of China (NSFC) (No. 51775432), the

Science and Technology Project of Weifang University of Science and Technology, China (No. 2018KJWZ08), and Facility Horticulture Laboratory of Universities in Shandong Program (No. 2018YY049).

References

[1] J. Hwang, C.-H. Park, W. Gao, and S.-W. Kim, "A three-probe system for measuring the parallelism and straightness of a pair of rails for ultra-precision guideways," *International Journal of Machine Tools and Manufacture*, vol. 47, no. 7-8, pp. 1053–1058, 2007.

[2] P. Zhang, Y. Chen, C. Zhang, J. Zha, and T. Wang, "Influence of geometric errors of guide rails and table on motion errors of hydrostatic guideways under quasi-static condition," *International Journal of Machine Tools and Manufacture*, vol. 125, pp. 55–67, 2018.

[3] J. Hu, C. Liu, Y. Guo, and X. Liang, "Static and dynamic characteristics of a hydrostatic guideway system based on electrorheological fluid," *Journal of Vibration and Shock*, vol. 35, no. 22, pp. 25–30, 2016.

[4] M. Masuko and T. Nakahara, "The influences of the fluid capacitance in the oil feed line system on the transient response of hydrostatic guideways," *International Journal of Machine Tool Design and Research*, vol. 14, no. 3, pp. 233–244, 1974.

[5] Z. Wang, W. Zhao, Y. Chen, and B. Lu, "Prediction of the effect of speed on motion errors in hydrostatic guideways," *International Journal of Machine Tools and Manufacture*, vol. 64, pp. 78–84, 2013.

[6] J. Lee, A. H. Ghasemi, C. E. Okwudire, and J. Scruggs, "A linear feedback control framework for optimally locating passive vibration isolators with known stiffness and damping parameters," *Journal of Vibration and Acoustics*, vol. 139, no. 1, article 011006, 2017.

[7] J. Lee and C. E. Okwudire, "Reduction of vibrations of passively-isolated ultra-precision manufacturing machines using mode coupling," *Precision Engineering*, vol. 43, pp. 164–177, 2016.

[8] D. Yoon and C. E. Okwudire, "Active assist device for simultaneous reduction of heat and vibration in precision scanning stages," *Precision Engineering*, vol. 46, pp. 193–205, 2016.

[9] A. Fakhar and R. Kolahchi, "Dynamic buckling of magnetorheological fluid integrated by visco-piezo-GPL reinforced plates," *International Journal of Mechanical Sciences*, vol. 144, pp. 788–799, 2018.

[10] R. Kishore, S. K. Choudhury, and K. Orra, "On-line control of machine tool vibration in turning operation using electromagneto rheological damper," *Journal of Manufacturing Processes*, vol. 31, pp. 187–198, 2018.

[11] Y. S. Tarng, J. Y. Kao, and E. C. Lee, "Chatter suppression in turning operations with a tuned vibration absorber," *Journal of Materials Processing Technology*, vol. 105, no. 1-2, pp. 55–60, 2000.

[12] J. Fei, B. Lin, S. Yan et al., "Chatter mitigation using moving damper," *Journal of Sound and Vibration*, vol. 410, pp. 49–63, 2017.

[13] A. H. H. Hosseinabadi and Y. Altintas, "Modeling and active damping of structural vibrations in machine tools," *CIRP Journal of Manufacturing Science and Technology*, vol. 7, no. 3, pp. 246–257, 2014.

[14] K. Mori, D. Kono, I. Yamaji, and A. Matsubara, "Vibration reduction of machine tool using viscoelastic damper support," *Procedia CIRP*, vol. 46, pp. 448–451, 2016.

[15] K. Mori, D. Kono, I. Yamaji, and A. Matsubara, "Modelling of viscoelastic damper support for reduction in low frequency residual vibration in machine tools," *Precision Engineering*, vol. 50, pp. 313–319, 2017.

[16] T. Aoyama and I. Inasaki, "Application of electrorheological fluid dampers to machine tool elements," *CIRP Annals*, vol. 46, no. 1, pp. 309–312, 1997.

[17] Z. H. Chen, *Study on Dynamics Performance of Linear Feed System with MR Damping*, Guangdong University of Technology, Guangzhou, China, 2008, in Chinese.

[18] M. Bayat and I. Pakar, "Nonlinear free vibration analysis of tapered beams by Hamiltonian approach," *Journal of Vibroengineering*, vol. 13, no. 4, pp. 654–661, 2011.

[19] I. Pakar, M. Bayat, and M. Bayat, "On the approximate analytical solution for parametrically excited nonlinear oscillators," *Journal of Vibroengineering*, vol. 14, no. 1, pp. 423–429, 2012.

[20] I. Pakar and M. Bayat, "Analytical study on the non-linear vibration of Euler-Bernoulli beams," *Journal of Vibroengineering*, vol. 14, no. 1, pp. 216–224, 2012.

[21] H. Tavakoli and S. Soleimani Kutanaei, "Evaluation of effect of soil characteristics on the seismic amplification factor using the neural network and reliability concept," *Arabian Journal of Geosciences*, vol. 8, no. 6, pp. 3881–3891, 2015.

[22] S. Rezaei, A. J. Choobbasti, and S. S. Kutanaei, "Site effect assessment using microtremor measurement, equivalent linear method, and artificial neural network (case study: Babol, Iran)," *Arabian Journal of Geosciences*, vol. 8, no. 3, pp. 1453–1466, 2015.

[23] N. M. Wereley, L. Pang, and G. M. Kamath, "Idealized hysteresis modeling of electrorheological and magnetorheological dampers," *Journal of Intelligent Material Systems and Structures*, vol. 9, no. 8, pp. 642–649, 1998.

[24] C. Graczykowski and P. Pawłowski, "Exact physical model of magnetorheological damper," *Applied Mathematical Modelling*, vol. 47, pp. 400–424, 2017.

[25] L. H. Wang, *Research on Nonlinear Dynamic Characteristics Identifition of NC Table*, Huazhong University of Science & Technology, Wuhan, China, 2009, in Chinese.

[26] L. H. Wang, R. S. Du, B. Wu, and S. Z. Yang, "Nonlinear dynamic characteristics of NC table," *China Mechanical Engineering*, vol. 20, no. 13, pp. 1513–1519, 2009, in Chinese.

[27] Q. Wu, *The Study on Dynamics Characteristics and Stability of Feed System in Big-Inertia*, Lanzhou University of Technology, Lanzhou, China, 2012, in Chinese.

[28] C. Duan and R. Singh, "Super-harmonics in a torsional system with dry friction path subject to harmonic excitation under a mean torque," *Journal of Sound and Vibration*, vol. 285, no. 4-5, pp. 803–834, 2005.

[29] C. Duan and R. Singh, "Dynamic analysis of preload nonlinearity in a mechanical oscillator," *Journal of Sound and Vibration*, vol. 301, no. 3–5, pp. 963–978, 2007.

[30] T. C. Kim, T. E. Rook, and R. Singh, "Super- and sub-harmonic response calculations for a torsional system with clearance nonlinearity using the harmonic balance method," *Journal of Sound and Vibration*, vol. 281, no. 3–5, pp. 965–993, 2005.

[31] X. Kong, W. Sun, B. Wang, and B. Wen, "Dynamic and stability analysis of the linear guide with time-varying, piecewise-nonlinear stiffness by multi-term incremental harmonic balance method," *Journal of Sound and Vibration*, vol. 346, pp. 265–283, 2015.

[32] O. T. Sen, J. T. Dreyer, and R. Singh, "Envelope and order domain analyses of a nonlinear torsional system decelerating

under multiple order frictional torque," *Mechanical Systems and Signal Processing*, vol. 35, no. 1-2, pp. 324–344, 2013.

[33] S. Wang, L. Hua, C. Yang, X. Han, and Z. Su, "Applications of incremental harmonic balance method combined with equivalent piecewise linearization on vibrations of nonlinear stiffness systems," *Journal of Sound and Vibration*, vol. 441, pp. 111–125, 2019.

[34] S. Zhou, G. Song, M. Sun, and Z. Ren, "Nonlinear dynamic analysis of a quarter vehicle system with external periodic excitation," *International Journal of Non-Linear Mechanics*, vol. 84, pp. 82–93, 2016.

[35] E. A. de Souza Neto and Y. T. Feng, "On the determination of the path direction for arc-length methods in the presence of bifurcations and 'snap-backs'," *Computer Methods in Applied Mechanics and Engineering*, vol. 179, no. 1-2, pp. 81–89, 1999.

[36] H. Wu, *Study on Nonlinear Dynamics of Tilting Pad Journal Bearing-Rotor System*, Harbin Institute of Technology, Harbin, China, 2007, in Chinese.

[37] Q. C. Zhang, H. L. Wang, Z. W. Zhu, F. Shen, A. D. Ren, and H. Y. Liu, *Theory and Application of Bifurcation and Chaos*, Tianjin University Press, Tianjin, China, 2005, in Chinese.

[38] P. Friedmann, C. E. Hammond, and T.-H. Woo, "Efficient numerical treatment of periodic systems with application to stability problems," *International Journal for Numerical Methods in Engineering*, vol. 11, pp. 1117–1136, 1997.

[39] W. Xu, *Numerical Analysis Methods for Stochastic Dynamical System*, Science Press, Beijing, China, 2013, in Chinese.